Topical Review published in the J. Phys.: Condens. Matter **16**, R1183-R1204 (2004)

Current-Induced Pair Breaking in Magnesium Diboride

Milind N. Kunchur*
Department of Physics and Astronomy
University of South Carolina, Columbia, SC 29208
(Dated: Received 21^{st} July 2004; published 19^{th} August 2004.)

The transport of electrical current through a superconductor falls into three broad regimes: non-dissipative, dissipative but superconducting, and normal or non-superconducting. These regimes are demarkated by two definitions of critical current: one is the threshold current above which the superconductor enters a dissipative (resistive) state; the other is the thermodynamic threshold above which the superconductivity itself is destroyed and the superconducting order parameter Δ vanishes. The first threshold defines the conventional critical current density j_c and the second defines the depairing (or pair-breaking) current j_d. Type II superconductors in the mixed state have quantized flux vortices, which tend to move when acted upon by the Lorentz driving force of an applied transport current. In such a mixed state the resistance vanishes only when vortices are pinned in place by defects and the applied current is below the threshold j_c required to overcome pinning and mobilize the vortices. Typically $j_d \gg j_c$ and a direct experimental measurement of j_d over the entire temperature range ($0 \leq T \leq T_c$) is prohibited by the enormous power dissipation densities ($p \sim 10^{10}$– 10^{12}W/cm^3) needed to reach the normal state. In this work, intense pulsed signals were used to extend transport measurements to unprecedented power densities ($p \sim 10^9 - 10^{10}$ W/cm^3). This together with MgB_2's combination of low normal-state resistivity (ρ_n) and high transition temperature (T_c) have permitted a direct estimation of j_d over the entire temperature range. This review describes our experimental investigation of current-induced depairing in MgB_2, and provides an introduction to the phenomenological theories of superconductivity and how the observations fit in their context.

PACS numbers: 74, 74.25.Sv, 74.25.Fy, 74.25.Bt
Keywords: Critical current, pair breaking, depairing, superconductor, superconductivity, flux, fluxon, vortex, magnesium diboride, mgb2

I. INTRODUCTION

When a superconductor is cooled below some transition temperature T_c, it undergoes a phase transition leading to the formation of a superconducting state wherein its charge carriers correlate and condense into a coherent macroscopic quantum state. In the superconducting state, the system expels magnetic flux upto magnetic field values below H_c, the thermodynamic field. In type II superconductors, the flux expulsion is partial for fields between the lower and upper critical fields, H_{c1} and H_{c2} respectively. The superconducting state is also characterized by an absence of resistivity for current densities j below some critical value j_c. In type II superconductors, there is partial resistivity for j values between j_c and j_d, where j_d is the pair-breaking or depairing current density[1].

The formation of this state is governed principally by a competition between four energies: condensation, magnetic-field expulsion, thermal, and kinetic. The order parameter Δ, that describes the extent of condensation and the strength of the superconducting state, is reduced as the temperature T, magnetic field H, and electric current density j are increased. The boundary in the T-H-j phase space that separates the superconducting and normal states is where Δ vanishes, and the three parameters attain their critical values $T_{c2}(H, j)$, $H_{c2}(T, j)$, and $j_d(T, H)$. j_d sets the intrinsic upper limiting scale for supercurrent transport in any superconductor.

Close to T_c, $j_d(T)$ has been investigated in several systems[1–3]. In a few materials[4,5], $j_d(T)$ has been measured down to about $0.2T_c$. Here we review our investigation of current-induced pair-breaking in MgB_2, which represents a complete ($0 \lesssim T \lesssim T_c$) investigation of j_d by a direct transport method.

II. THEORETICAL BACKGROUND

The magnitude and temperature dependence of the pair-breaking current density can be adequately described by phenomenological theories of superconductivity, such as the London theory and the Ginzburg-Landau (GL) theory. In a microscopic theory such as the Bardeen-Stephen-Cooper (BCS) theory, experimental quantities are calculated from microscopic parameters such as the strength of the effective attractive interaction that leads to Cooper pair formation and the density of states at the Fermi level. Often these microscopic parameters are not sufficiently well known. In phenomenological theories, connections are made between the differ-

[1] Type I superconductors can also exhibit partial resistivity in the superconducting state because of fluctuations, presence of a large ($H > H_c$) current induced self field at the surface (Silsbee's rule), phase slippage as one approaches the phase boundary, or motion of magnetic domains in the intermediate state.

ent observables from contraints based on thermodynamic principles and electrodynamical properties of the superconducting state. Below we give a simplified introduction to the different theoretical approaches for estimating the depairing current density and its temperature dependence.

A. London theory

1. Basic framework

The London theory[6] of superconductivity provides a description of the observed electrodynamical properties by supplementing the basic Maxwell equations by additional equations, which contrain the possible behavior to reflect the two hallmarks of the superconducting state—perfect conductivity and Meissner effect. Note that these properties hold only partially when mobile vortices are present.

An ordinary metal (normal conductor) requires a driving electric field E to maintain a constant current against resistive losses. In the simple Drude picture, this produces Ohm's law behavior, $j = \sigma E$, with a conductivity given by $\sigma = ne^{*2}\tau/m^*$, where n is the number density of charge carriers, and e^* and m^* are their effective charge and mass respectively.

A superconductor can carry a resistanceless current and so an electric field is not required to carry a persistent current. Instead E in a perfectly conducting state causes a ballistic acceleration of charge so that $\partial j/\partial t \propto E$. If the number density of effective charge carriers (pairs) participating in the supercurrent is n_s^*, then $j = n_s^* e^* v_s$, where v_s is the carrier (superfluid) velocity, and

$$E = \left(\frac{m^*}{n_s^* e^{*2}}\right)\frac{\partial j}{\partial t}. \tag{1}$$

This is the first London equation, which reflects the dissipationless acceleration of superfluid.

The second property that needs to be accounted for is the expulsion of magnetic flux by a superconductor. The magnetic field is exponentially screened from the interior and hence follows a spatial dependence

$$\nabla^2 H = H/\lambda^2, \tag{2}$$

where λ is a screening length called the London penetration depth. Together with the Maxwell equation $\nabla \times H = 4\pi j/c$, this implies the following condition between H and j:

$$H = -\left(\frac{4\pi\lambda^2}{c}\right)(\nabla \times j). \tag{3}$$

This is the second London equation and it describes the property of a superconductor to exclude magnetic flux from its interior. The prefactors in the two London equations are related through the Maxwell equations. Taking the curl of both sides of Eq. 1 and replacing $\nabla \times E$ on the left side with $-\frac{1}{c}\frac{\partial H}{\partial t}$ and substituting for $\nabla \times j$ on the R.H.S. with Eq. 3 gives the expression for the penetration depth as

$$\lambda = \sqrt{m^* c^2/4\pi n_s^* e^{*2}} = \sqrt{mc^2/4\pi n_s e^2}, \tag{4}$$

where the pair quantities with asterisks have been replaced with their more common single-carrier counterparts ($2n_s^* = n_s$, $e^* = 2e$, and $m^* = 2m$) in the last step[2]. In the MKSA (SI) system, Eq. 4 becomes $\lambda = \sqrt{10m^*/4\pi n_s^* e^{*2}}$.

A third relationship of importance in the discussion of the pair-breaking current concerns the thermodynamic critical field H_c. When flux is expelled, the free energy density is raised by the amount $H^2/8\pi$. The critical flux expulsion energy (for the ideal case of a type I superconductor with a non-demagnetizing geometry and dimensions large compared to the penetration depth) corresponds to the condition

$$f_c = f_n - f_s = H_c^2/8\pi \tag{5}$$

where the L.H.S. of the equation represents the condensation energy—the difference in free energy densities $f_n - f_s$ between the normal and superconducting states.

2. Depairing current density in the London framework

We now have all the ingredients we need to obtain the usual London estimate of the depairing current density. Taking j_d to represent the condition when the kinetic energy density equals the condensation energy, we have $\frac{1}{2}n_s^* m^* v_s^2 = \frac{1}{2}m^* j_d^2/(n_s^* e^*)^2 = f = H_c^2/8\pi$. Substituting for λ (Eq. 4) then gives the required expression for the depairing current density

$$j_d = \frac{cH_c}{4\pi\lambda}. \tag{6}$$

In practical MKSA units, Eq. 6 can be written as $j_d = (10^7/4\pi)(B_c/\lambda)$, where j_d is in A/m^2, B_c is the thermodynamic critical flux density in Teslas and λ is the penetration depth in meters.

Note that this derivation assumed that n_s remains unchanged as j approached j_d. In reality n_s diminishes as the superconductivity is destroyed and the normal phase boundary is approached. Hence Eq. 6 will be an overestimate for j_d.

[2] In subsequent expressions we retain the asterisk marked quantities in our notation to maintain generality. This allows, for example, the inclusion of band-structure effects on the effective mass so that a more exact value of m^* can be used rather than simply taking the $m^* = 2m$ corresponding to the free-electron model.

B. Ginzburg-Landau theory

1. Basic framework

There are situations where a system's quantum wavefunction cannot be solved for by usual means because the Hamiltonian is unknown or not easily approximated. The GL formulation is a clever construction that allows useful information and conclusions to be extracted in such a situation where one cannot solve the problem quantum mechanically. For describing macroscopic properties—such as j_d that we are about to calculate—the GL theory is in fact more amenable than the microscopic theory.

The idea is to introduce a complex phenomenogical order parameter (pseudowavefunction) $\psi = |\psi|e^{i\varphi}$ to represent the superconducting state. $|\psi(r)|^2$ is assumed to approximate the local density of superconducting charge carriers $n_s(r)$. The free energy density f_s of the superconducting state is then expressed as a reasonable function of $\psi(r)$ plus other energy terms. A "solution" to $\psi(r)$ is now obtained by the minimization of free energy rather than through quantum mechanics. The unknown parameters of the theory are then solved in terms of measurable physical quantities thereby providing contraints between the different quantities of the superconducting state.

Close to the phase boundary, $|\psi|^2$ is small and so f_s can be expanded keeping the lowest two orders of $|\psi|^2$. First let us consider the simplest situation where there are no currents, gradients in $|\psi|$, or magnetic fields present. Then we have

$$f_s = f_n + \alpha|\psi|^2 + \frac{\beta}{2}|\psi|^4, \tag{7}$$

where α and β are temperature dependent coefficients whose values are to be determined in terms of measurable parameters. The coefficients can be determined as follows. First of all for the solution of $|\psi|^2$ to be finite at the minimum free energy, β must be positive. Second, for the solution of $|\psi|^2$ to be non-zero, α must be negative. Since $|\psi|^2$ vanishes above T_c, α must change its sign upon crossing T_c. The minimum in f_s occurs at

$$|\psi|^2 = -\alpha/\beta. \tag{8}$$

Substituting this back in Eq. 7 and using the definition of H_c (Eq. 5), Eq. 8 can be recast as

$$f_c = \frac{H_c^2}{8\pi} = \frac{\alpha^2}{2\beta} \tag{9}$$

giving one of the connections between α and β and a measurable quantity (H_c). A second connection can be obtained by noting that n_s^* in Eq. 4 can be replaced by $|\psi|^2$, taking it's equilibrium value from Eq. 8

$$\lambda^2 = \frac{m^*c^2}{4\pi|\psi|^2e^{*2}} = \frac{-\beta}{\alpha}\left(\frac{m^*c^2}{4\pi e^{*2}}\right). \tag{10}$$

Solving Eqs. 9 and 10 simultaneously gives the GL coefficients:

$$\alpha = -\frac{e^{*2}}{m^*c^2}H_c^2\lambda^2 \qquad \text{and} \qquad \beta = \frac{4\pi e^{*4}}{m^{*2}c^4}H_c^2\lambda^4 \tag{11}$$

Next, the effect of fields and currents can be included in Eq. 7 by adding terms corresponding to the field energy density and kinetic energy of the current:

$$\begin{aligned} -f_c &= \alpha|\psi|^2 + \frac{\beta}{2}|\psi|^4 + \frac{1}{2}|\psi|^2 m^* v_s^2 + \frac{H^2}{8\pi} \\ &= \alpha|\psi|^2 + \frac{\beta}{2}|\psi|^4 + \frac{1}{2m^*}\left|\left(\frac{\hbar}{i}\nabla - \frac{e^*}{c}A\right)\psi\right|^2 + \frac{H^2}{8\pi} \end{aligned} \tag{12}$$

where $\boldsymbol{v}_s$ is the superfluid velocity. If the amplitude $|\psi|$ is constant and only its phase φ varies spatially, then $\boldsymbol{v}_s = (\frac{\hbar\nabla\varphi}{m^*} - \frac{e^*\boldsymbol{A}}{cm^*})$. Also in the situation of interest to us—currents of pair-breaking level—the gradient term is much larger than the A term in the operator for velocity. In this case $\boldsymbol{v}_s \approx \frac{\hbar\nabla\varphi}{m^*}$.

It should be noted that the above derivation assumed proximity to T_c only for the purpose that $|\psi|$ be small so that f_s could be represented as a limited power series expansion. In "dirty" superconductors—superconductors with a high impurity scattering rate—the approximate validity of the GL expressions extends down to $T \ll T_c$. In general, the expressions should be valid at all T as long as $|\psi|$ is small and the proper temperature dependent values of α and β are used, as expressed through the temperature dependencies of H_c and λ. The treatment thus far assumes that charge carriers from only one band contribute to the superconductivity, i.e., it is a SBGL (single-band Ginzburg-Landau) theory.

2. Depairing current density in the SBGL framework

We can now derive j_d by finding the value of j above which $|\psi|$ vanishes. First we consider the case when $H = 0$. We will assume j to be uniform across the cross section. We will justify this assumption later and look in detail at the conditions when the assumption is valid. Eq. 12 then simplifies to

$$-f_c = \alpha|\psi|^2 + \frac{\beta}{2}|\psi|^4 + \frac{1}{2}|\psi|^2 m^* v_s^2. \tag{13}$$

For zero v_s, we saw earlier (Eq. 8) that the equilibrium value of $|\psi|^2$ that minimizes the free energy is $|\psi_\infty|^2 = -\alpha/\beta$. For a finite v_s minimization of Eq. 13 gives

$$|\psi|^2 = \frac{-\alpha}{\beta}\left(1 - \frac{m^* v_s^2}{2|\alpha|}\right) \tag{14}$$

with the corresponding supercurrent density

$$j = e^*|\psi|^2 v_s = \frac{-e^*\alpha}{\beta}\left(1 - \frac{m^* v_s^2}{2|\alpha|}\right) v_s. \tag{15}$$

The maximum possible value of this expression can now be identified with j_d:

$$j_d(T) = \frac{-2e^*\alpha}{3\beta}\left(\frac{2|\alpha|}{3m^*}\right)^{1/2} = \frac{cH_c(T)}{3\sqrt{6}\pi\lambda(T)} \tag{16}$$

where the GL-theory parameters were replaced by their expressions in terms of the physical measurables H_c and λ through Eqs. 11.

The approximate temperature dependence of j_d can be obtained by inserting the generic empirical temperature dependencies $H_c(T) \approx H_c(0)[1-(T/T_c)^2]$ and $\lambda(T) \approx \lambda(0)/\sqrt{[1-(T/T_c)^4]}$ giving

$$j_d(T) \approx j_d(0)[1-(T/T_c)^2]^{\frac{3}{2}}[1+(T/T_c)^2]^{\frac{1}{2}} \tag{17}$$

where

$$j_d(0) = cH_c(0)/[3\sqrt{6}\pi\lambda(0)] \tag{18}$$

is the zero-temperature depairing current density. In practical MKSA units, Eq. 18 can be written as $j_d(0) = 10^7 \times B_c(0)/[3\sqrt{6}\pi\lambda(0)]$, where j_d is in A/m^2, B_c is in T and λ is in m.

For the dirty case, instead of Eq. 17, the temperature dependence of Eq. 16 can be better approximated as[1,4]

$$j_d(T) \approx j_d(0)[1-(T/T_c)^2]^{\frac{3}{2}}. \tag{19}$$

Usually H_c can't be measured reliably, but from the relation

$$H_c = \sqrt{\frac{\Phi_0 H_{c2}}{4\pi\lambda^2}} \tag{20}$$

Eq. 18 can be recast as

$$j_d(0) = \sqrt{\frac{c^2\Phi_0}{216\pi^3}}\left(\frac{\sqrt{H_{c2}(0)}}{\lambda^2(0)}\right), \tag{21}$$

which in MKSA becomes $j_d(0) = 5.56\times10^{-3}\times\sqrt{B_{c2}(0)}/\lambda^2(0)$, where j_d is in A/m^2, B_{c2} is the upper critical flux density in Teslas and λ is in meters.

Close to T_c, Eq. 17 reduces to $j_d(T\approx T_c) \approx 4j_d(0)[1-T/T_c]^{\frac{3}{2}}$. This can be inverted to give the shift in transition temperature $T_{c2}(j)$ at small currents, with the well-known $j^{2/3}$ proportionality:

$$1-\frac{T_{c2}(j)}{T_c} \approx \left(\frac{1}{4}\right)^{\frac{2}{3}}\left[\frac{j}{j_d(0)}\right]^{\frac{2}{3}}, \tag{22}$$

where $T_c \equiv T_{c2}(0)$. Note that if heat removal from the sample is ineffective, Joule heating will give an apparent shift $\Delta T_c \propto \rho j^2$, which is the cube of the intrinsic $\sim j^{2/3}$ depairing shift near T_c. Hence Joule heating is easily distinguishable from a pair-breaking shift. (The preceding discussion is based on Refs. 7 and 1.)

C. GL formulation for a two-band superconductor

We now consider the two-band Ginzburg-Landau (2BGL) applicable to a system such as MgB_2 where two bands contribute to condensates. In this case, the condensation energy density can be expressed as[8–10]

$$\begin{aligned}-f_c = &\left\{\alpha_1|\psi_1|^2+\frac{\beta_1}{2}|\psi_1|^4+\frac{1}{2m_1^*}\left|\left(\frac{\hbar}{i}\nabla-\frac{e^*}{c}A\right)\psi_1\right|^2\right\}\\ &+\left\{\alpha_2|\psi_2|^2+\frac{\beta_2}{2}|\psi_2|^4+\frac{1}{2m_2^*}\left|\left(\frac{\hbar}{i}\nabla-\frac{e^*}{c}A\right)\psi_2\right|^2\right\}\\ &+\left\{\epsilon[\,\psi_1^*\psi_2+c.c.]\right\}+\left\{\frac{H^2}{8\pi}\right\}\end{aligned} \tag{23}$$

where the first two braces correspond to the free energy contributions of the condensates of each band and the third term corresponds to the interband interaction energy.

As before, for the case of no applied field and uniform current distribution, this simplifies to

$$\begin{aligned}-f_c = &\left\{\alpha_1|\psi_1|^2+\frac{\beta_1}{2}|\psi_1|^4+\alpha_2|\psi_2|^2+\frac{\beta_2}{2}|\psi_2|^4\right\}\\ &+\frac{1}{2}\left\{\,|\psi_1|^2m_1^*v_{s1}^{*2}+|\psi_2|^2m_2^*v_{s2}^{*2}\right\}+\epsilon\left\{\,\psi_1^*\psi_2+c.c.\right\}\end{aligned} \tag{24}$$

The phases of the two condensates are locked together since at equilibrium the interband free energy is minimized when $\cos(\phi_1-\phi_2)=1$ or -1 (for $\epsilon<0$ and $\epsilon>0$ respectively). Hence the superfluid momenta are equal, $m_1^*v_1^* = m_2^*v_2^*$, and the superfluid velocities, v_1^* and v_2^*, will be similar to the extent that the effective masses are similar.

Because of the rather large number of parameters in Eq. 24, it is not very meaningful to derive an expression for j_d for direct quantitative comparison with the experimental data. Rather we will take the SBGL expression for j_d in Eq. 16 and insert the actual measured temperature dependencies of H_c and λ. We expect those empirical temperature dependencies to account for modifications due to the presence of two bands. As will be seen below, the experiment confirms this contention. Note that for current flow in the *ab* plane (which is our experimental situation) the stronger planar π band provides the main contribution to $\jmath_s$. In this case the behaviour should qualitatively follow SBGL with the appropriately modified parameters.

D. Depairing current from quasiparticle-energy shift

In the previous derivations in the framework of phenomenological theories, no account was taken of the superconducting gap. As a final step in obtaining theoretical estimations of j_d, let us consider how the supercurrent is limited because of its effect on the superconducting

gap. Unlike the GL treatments, this one is particularly applicable to the $T \ll T_c$ regime. In the microscopic theory, the superfluid density does not decline continuously as j and v_s are increased. Rather, n_s remains roughly constant until v_s reaches its depairing value[1,7]

$$v_d = \frac{\Delta}{\hbar k_F} = \frac{2\hbar}{\pi m^* \xi_0}, \tag{25}$$

which corresponds to the point when the shift, $\hbar \boldsymbol{k}_F.\boldsymbol{v}_s$, in the quasiparticle energies (QPE) equals the gap causing the gap to vanish for those states. In Eq. 25, ξ_0 is the intrinsic BCS coherence length. The value of ξ deduced from the upper critical field will be a lower bound on ξ_0 since scattering reduces the effective ξ (in the dirty-limit $\xi \approx \sqrt{\xi_0 l}$, where l is the mean-free path[7]). j remains closely proportional to v_s until v_d, then n_s drops precipitously so that the maximum current is only slightly (2%) higher than the value when v_s=v_d. Thus to a good approximation $j_d \simeq e^* n_s^* v_d$. Combining this with Eq. 25 gives

$$j_d \simeq \frac{m^* c^2 \Delta}{4\pi e^* \lambda^2 \hbar k_F} \simeq \frac{c^2 \hbar}{2\pi^2 e^* \lambda^2 \xi_0}. \tag{26}$$

The first R.H.S. involves the parameters such as Δ and k_F whose absolute values are not known accurately but whose temperature dependencies are well established, since k_F is of course constant and the gaps have a temperature dependence that is well described by the standard BCS function[11,12]. Hence from the first R.H.S. we determine the temperature dependence of j_d as

$$j_d(T) = j_d(0) \left(\frac{\lambda^2(0)}{\Delta(0)} \right) \frac{\Delta(T)}{\lambda^2(T)}. \tag{27}$$

On the other hand, the second R.H.S. of Eq. 26 involves parameters such as ξ_0 whose absolute magnitude is better known (from measurements of H_{c2} and the relation $H_{c2} = \Phi_0/2\pi\xi^2$). Hence we use the second R.H.S. of Eq. 26 to estimate the absolute magnitude of $j_d(0)$ as

$$j_d(0) = \left(\frac{c^2 \Phi_0}{8\pi^5} \right)^{\frac{1}{2}} \frac{\sqrt{H_{c2}(0)}}{\lambda^2(0)}, \tag{28}$$

which in MKSA becomes $j_d(0) = 9.19 \times 10^{-3} \times \sqrt{B_{c2}(0)}/\lambda^2(0)$.

E. Microscopic calculation

Various authors have calculated $j_d(T)$ from a microscopic basis[1,13,14]. For arbitrary temperatures and mean free paths, one must use the Gorkov equations as the starting point. Kupriyanov and Lukichev[15] have derived $j_d(T)$ from the Eilenberger equations, which are a simplified version of the Gorkov equations. This derivation is beyond the scope of the present review, but a nice shortened version can be found in reference 4. The microscopic calculation confirms the overall temperature dependence predicted by GL and the two normalized curves differ only slightly from each other (e.g., see Fig. 4 of reference 4).

F. Comparison between different theoretical estimates

We will now compare the different theoretical estimates of $j_d(0)$ obtained by the different approaches and calculate their relative ratios from Eqs. 6, 18, 21, and 28. The London estimate, as discussed earlier, should be an overestimate. Its value is 1.84 times higher than the GL estimate. Similarly, the estimate from QPE shift turns out to be 1.65 times higher than GL. Since the QPE shift calculation is based on a simple single isotropic gap, the actual $j_d(0)$ will be different and somewhat lower. For the very dirty ($l \ll \xi_0$) and very clean ($l \gg \xi_0$) limits, the actual $j_d(0)$ is expected to be 0.67 and 0.82 times the London estimate respectively[1]. Hence these estimates should be correct at most to a factor-of-two accuracy. Errors in the values of the parameters will further add to the inaccuracy of the calculated value. So when comparing with the experiment, an agreement to within half an order of magnitude is about the best that can be expected.

III. EXPERIMENTAL METHODS

A. Samples

The samples are 400nm-thick c-axis oriented films of MgB_2 on sapphire. In this paper we show data on four bridges, labelled S, M, N, and L with lateral dimensions 2.8 x 33, 3.0 x 61, 3.0 x 60, and 9.7 x 172 μm^2 respectively. The lateral dimensions are uncertain by $\pm 0.7 \mu$m and the mean thickness by ± 50 nm. TEM (transmission electron microscopy) shows variations in thickness of about $\delta t/t \sim 10\%$. The films were fabricated using a two-step method whose details are described elsewhere[16,17]. An amorphous boron film was deposited on a $(1\bar{1}02)$ Al_2O_3 substrate at room temperature by pulsed-laser ablation. The boron film was then put into a Nb tube with high-purity Mg metal (99.9%) and the Nb tube was then sealed using an arc furnace in an argon atmosphere. Finally, the heat treatment was carried out at 900° C for 30 min. in an evacuated quartz ampoule sealed under high vacuum. X-ray diffraction indicates a highly c-axis-oriented crystal structure normal to the substrate with undetectable impurity phases. Magnetization $M(T)$ curves have a λ-limited transition width of 1.5K (T_c-spread < 0.2K). However, the aforementioned variations in thickness produce a broadening of $R(T)$ with increasing j. The films were photolithographically patterned down to narrow bridges and in the case of one sample (N) the lead areas were further delineated by mechanical scribing.

The samples have a normal-state resistivity at room temperature $\rho_n(300\text{K}) \approx 14\mu\Omega$-cm, which is about 7 times that found in clean single crystals[18]. The enhancement appears to to be due to microscopic disorder (scattering) and not just some extra series resistance at grain boundaries, since H_{c2} is also enhanced by about the same factor over its values in single crystals[18,19]. Also measurements of λ on these films show no evidence of grain-boundary weak-linked behaviour, which would be manifested as a non-linearity in response and as an increase in the apparent absolute magnitude of λ, which were not observed[20].

B. Cryogenics

Two sets of apparatus were used for the measurements. Samples S, M, and L were measured in an Oxford Instruments$^{(R)}$ liquid-helium based vapour-flow cryostat with a 16 Tesla superconducting magnet. Sample N was measured in a Cryomech$^{(R)}$ pulsed-tube closed-cycle refrigerator and a water-cooled copper magnet. In the latter case, the "zero field" could be made very small (< 0.7 G) by shielding the sample region using mu-metal. Lakeshore$^{(R)}$ diode and cernox sensors were employed for the thermometry.

C. Electrical measurements

Low-current resistance measurements ($I < 50\mu$A) were made by the standard four-probe DC technique. Higher current measurements were carried out using a pulsed technique with a four-probe configuration. A pulsed signal source (capable of both constant-current and constant-voltage modes) drives the signal through the sample and a series standard resistor R_{std}. The signals across the sample and R_{std} are then detected with a digital-storage oscilloscope. The temporal reproducibility of the system is ∼1 ns as can be evidenced from Fig. 1, which shows two sets of measurements of $I(t)$ and $V(t)$. The relative delay between rising edges of $I(t)$ and $V(t)$ corresponds approximately to the extra length of wires divided by the speed of light.

Pulse durations range 0.1–4 μs with a duty cycle of about 1 ppm. About 100 pulses are averaged to reduce the noise. A typical pair of current and voltage pulses is shown in Fig. 2. The values of I and V used in subsequent analyses correspond to the flat plateaus of the pulse waveforms. As these are time independent, the measurement corresponds effectively to a DC measurement albeit over a shorter-than-usual duration. The computed $R(t) = V(t)/I(t)$, shown in Fig. 2, is seen to have a 50 ns rise time. The total duration of the pulse is not relevant but the time at which the voltage or current is measured since it turns on. Since the signals saturate to well defined values by ∼100 ns, this is the effective dissipation time τ that is relevant to the thermal calculations

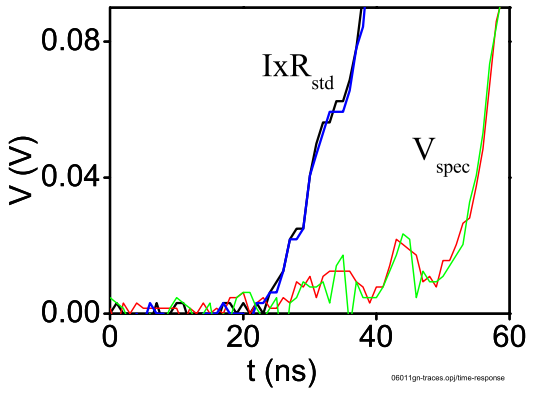

FIG. 1: Rising edges of voltage and current (voltage across R_{std}) across an MgB_2 bridge (sample N). The sample is in the normal state at room temperature. The graph contains two sets of measurements of $I(t)$ and $V(t)$ showing overlap and temporal reproducibility to within about 1 ns.

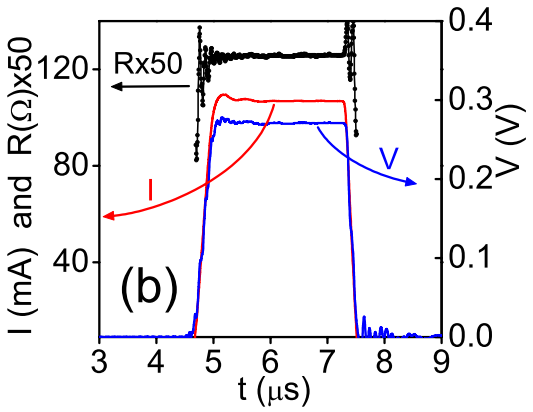

FIG. 2: Pulse waveforms at high dissipation levels ($j = 9.7$ MA/cm^2, $E = 83$ V/cm, and $p = jE = 803$ MW/cm^3 on the plateaus). The measurement was done on an MgB_2 bridge (sample S) just above T_c (at 42K). The resistance rises to (90% of) its final value in about 50 ns from the (10%) onset of I.

below. Some additional information on the electrical-measurement setup can be found in a previous review article[21] and other recent papers[22,23].

D. Heat conduction during pulsed measurements

We now look in more detail at the thermal processes involved in the removal of heat from the sample[24,25]. Heat generated in the film diffuses toward the interface with the substrate essentially instantaneously. On the time scale of nanoseconds, phonons transfer heat across the interface between the film and substrate. Heat then diffuses within the substrate in a matter of microseconds and finally into the heat sink in milliseconds. Thus for pulses of microsecond or shorter duration, the heat doesn't leave the substrate and for low duty cycles the thermometer will not register a temperature rise. The sample temperature rise is then composed of a tempera-

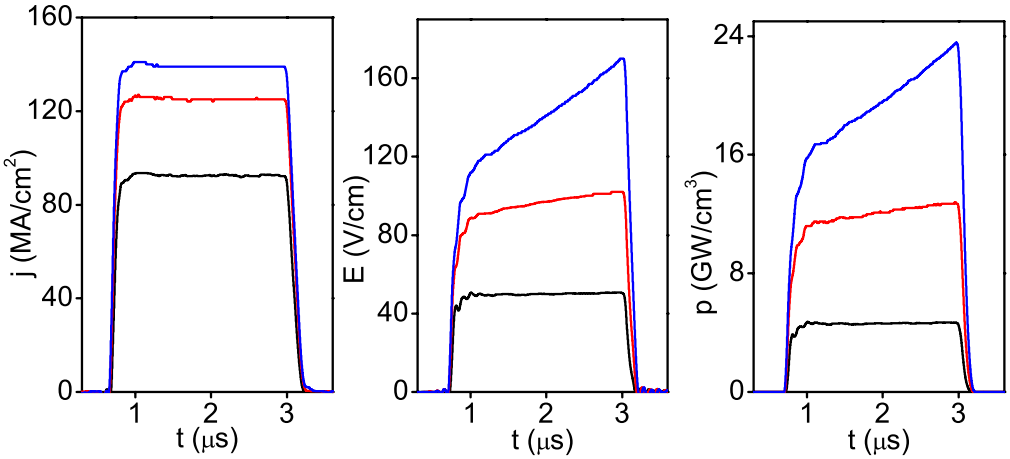

FIG. 3: Pulse waveforms showing a time-dependent temperature rise at extreme dissipation levels ($p > 10^{10}$ W/cm^3). The measurement was made on a 100 nm thick $Y_1Ba_2Cu_3O_7$ film on $LaAlO_3$[22,23] at T=50 K and B=10 T. The left, middle, and right panels show the current density, electric field, and power-dissipation density respectively.

ture gradient within the film, an abrupt temperature difference across the boundary, and a gradient within the substrate. Each can be expressed as an additive component of the thermal resistance R_{th}, which we will define as the temperature rise ΔT per unit power density p.

The temperature variation within the film given by $\Delta T_1(z) \simeq (p/\kappa_f)(tz - z^2/2)$ where $(t - z)$ is the distance of a point within the film from the interface, t is the film thickness and κ_f is the thermal conductivity of the film. Expressed as a thermal resistance this becomes

$$R_{th1}(z) \simeq \frac{1}{\kappa_f}\left(tz - \frac{z^2}{2}\right). \tag{29}$$

For MgB_2, κ_f = 0.1 and 0.4 W/K.cm at 10 K and 40 K respectively[26,27]. This yields an average R_{th} in the midplane of the film (i.e., at $z = t/2$) of 6 nK.cm^3/W at 10K and 1.5 nK.cm^3/W near T_c.

Phonon mismatch at the interface between film and substrate produces an abrupt temperature drop $\Delta T_2 = ptR_{bd}$, where R_{bd} is the thermal boundary resistance at the film-substrate interface. This can be expressed as a second component to R_{th}:

$$R_{th2} = tR_{bd}. \tag{30}$$

Most metallic films on sapphire exhibit the approximate empirical rule[28] $R_{bd}T^3 \approx 20$ cm^2.K^4/W. Thus $R_{th2} \sim 12$ nK.cm^3/W at 40 K (near T_c) and ~800 nK.cm^3/W at 10 K. (Ceramic on ceramic boundaries, such a $Y_1Ba_2Cu_3O_7$ on $LaAlO_3$, seem to fair better in this respect.)

Finally as the heat pulse propagates through the substrate, there is a third component to R_{th}, which for the long rectangular strip geometry is given by[25]:

$$R_{th3} = \frac{2.26t\tau w}{2(D_s\tau)^{1/2}[4(D_s\tau)^{1/2} + w]c_s}, \tag{31}$$

where $D_s = \kappa_s/c_s$ is the diffusion constant, κ_s and c_p are the thermal conductivity and specific heat of the substrate material, w is the width of the bridge, and τ is the duration for which the power is applied. For sapphire, $c_s \sim 3.2$ J/K.cm^3[29] and $\kappa \approx 10$ and 100 W/cm.K at 10 K and 40 K respectively[30]. Thus $D_s = \kappa_s/c_s \sim 3$ and 30 cm^2/s at 10 and 40 K respectively. This gives a thermal diffusion lengths $\sqrt{D\tau}$ within the substrate of 6–17 μm for T=10–40 K, for τ = 100 ns. Since our bridge widths (~2–10 μm) are small or comparable to these diffusion lengths, the denominator $\sim 8D\tau c_s \propto \kappa_s$ is mainly dependent on the conductivity of the substrate and is relatively independent of its specific heat. From Eq. 31 the last component of the thermal resistance then has an estimated magnitude of $R_{th3} \sim 0.8$–0.1 nK.cm^3/W in the T range 10–40 K respectively for a 3 μm wide bridge.

From the above estimated components, we can obtain the total thermal resistance

$$R_{th} = R_{th1} + R_{th2} + R_{th3} \tag{32}$$

as $R_{th} = 1.5 + 10 + 0.1 \approx 12$ nK.cm^3/W near T_c and 0.8 μK.cm^3/W at 10 K, where the dominating term comes from the boundary resistance.

E. Adiabatic heating

The worst-case scenario for sample heating is when the timescales and conditions are such that none of the generated heat escapes. In this case the energy density $p\tau$ dumped by the pulse will go entirely into raising the internal energy U. The temperature rise can then be expressed in terms of the film's specific heat as

$$p\tau = \delta U = \int_{T_0}^{T'} c(T)dT \approx c\Delta T, \tag{33}$$

where the last approximation applies for small temperature shifts, $c \equiv c(T_0)$ is the specific heat at the nominal bath temperature T_0, and T' is the final raised temperature, i.e., $\Delta T = T' - T_0$. The effective thermal resistance

in this case is

$$R_{thA} = \tau / c(T_0). \quad (34)$$

Close to T_c, $c(40\text{K}) \approx 0.044$ J/K.cm^3 in MgB_2[31]. For times between 100ns and 1μs after current turn on, the corresponding adiabatic R_{th} then has values in the range $\sim$2–20 μK.cm^3/W. Note that the R_{thA} values are about three orders of magnitude higher than when there is heat conduction (Eq. 32) but place an absolute upper limit on the actual R_{th}. Because R_{thA} is directly proportional to τ, the amount of heating can be made almost arbitrarily small by reducing the duration of the signal (for very short durations there will be addional corrections when the electrons can no longer equilibrate with the phonons). The above estimates were for $T \sim T_c$, at 5K the corresponding R_{thA} values will be one or two orders of magnitude higher.

F. Heat generation at contacts

As seen above, pulsed measurements greatly reduce the effective thermal resistance and accompanying temperature rise in the sample. In addition they can essentially eliminate problems associated with heat produced at lead contacts. This is because the contacts are typically located several mm away from the active part of the sample (the bridge) involved in the four-probe measurement. This distance is typically large compared to the thermal diffusion distance $\sqrt{D\tau}$. The specific heat at 10 K and 40 K is 1,400 and 50,000 J/K.m^3 respectively[31,32]. Together with the values of 10 and 40 W/m.K for thermal conductivity[26,27] gives diffusion constants of 0.007 and 0.0008 m^2/s at the two temperatures. Thus for dissipation durations 0.1–1 μs and temperatures 10–40 K, we get diffusion distances in the 9–84 μm range, which are about a hundred times shorter than the distance to the bridge. So heat generated at the contacts does not interfere with the measurement.

G. Pulse waveform distortion due to temperature rise

The third component of the thermal resistance R_{th3} arising from the flow of heat into the substrate is time dependent (Eq. 31). As a result intense heating can cause the resistance to rise with time and hence the voltage pulse becomes sloped[21]. Fig. 3 shows an example of this situation, where the measurements were done on $Y_1Ba_2Cu_3O_7$ films. Even in the case of a system with a relatively T independent ρ_n such as the MgB_2 films, in the superconducting state the flux-flow resistivity is T dependent, especially in the regime near T_c.

For very short pulses and/or low enough power densities, the temperature rise in the substrate $\Delta T = pR_{th3}$ becomes negligible and the main bottle neck for heat conduction becomes the thermal boundary resistance. If these conditions are satisfied the voltage pulse should appear flat. This was verified in all of our measurements and data was only taken when the pulses were undistorted as in Fig. 2. Note that the power-dissipation densities for the pulses in Fig. 3 are much higher than the levels used in the present work on MgB_2.

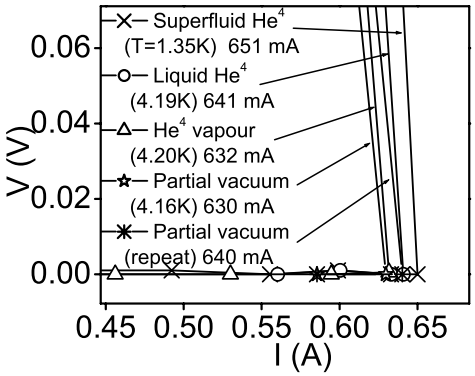

FIG. 4: IV curves for sample L at the lowest temperatures with the exposed surface of the film in contact with different thermal environments as indicated. The influence of thermal environment on Joule heating is seen to be minimal as there is no major systematic change in the threshold current at which the jump in voltage occurs.

H. Influence of thermal environment

In measurements involving a continuous DC signal or long time scales, substantial overall heating can be alleviated by immersing the sample directly in a liquid cryogen. This is especially noticeable when the cryogen is in a superfluid state[33]. In our measurements the timescales are such that even the substrate does not experience a sigificant rise in T. In this case we would expect that additional heat removal from the exposed surface of the film to a cryogen to not make a big difference. This is indeed the case as can be seen in Fig. 4 where IV curves measured in different thermal environments show a jump to the normal state at a value of I_d that is roughly independent of the thermal environment.

I. Electron-phonon disequilibrium

Beside macroscopic heating of the sample, other exotic situations can arise where the electronic temperature is significantly raised with respect to the phonons, which remain in equilibrium with the bath[23,34–45]. The characteristic time for the relaxation of energy between the electrons and phonons is typically under 10^{-8} s. This effect happens mainly when there is vigorous vortex motion and is not a main concern in the present work.

J. Temperature rise and thermal runaway

Except in the case when the sample has perfect electrical conductivity, in the dissipative state the measurement is necessarily accompanied by some rise in sample temperature. This leads to the risk of thermal runway, where a small temperature rise leads to increased dissipation, leading to a further temperature rise and so on. The sample can end up at a temperature much higher than the bath temperature and possibly in the normal state. If this scenario is fulfilled, the quantity actually measured will be the conventional j_c, demarkating the onset of dissipation, rather than the true j_d. The match needed to light a thermal runaway is flux-flow dissipation whose power density is given by $p_f \lesssim j^2\rho_n B/H_{c2}$. A small localized hot spot will not sustain a runaway since the current can simply avoid the hot spot and flow through more conductive regions. Also heat produced at one point does not remain localized on the timescale of the measurement but spreads uniformly across the width of the film because the thermal diffusion length, calculated earlier, is larger than the bridge width. Thus the the relevant parameter is the average dissipation across the sample volume.

At 10 K, this p_f is about 1.2 W/cm^3 taking an average self field of 100 G (all measurements here were made in zero applied magnetic field with the sample chamber shielded by mu-metal in some cases). From the R_{th} calculated earlier, this results in $\Delta T \approx 1.1$ K, which increases the sample resistance only marginally (ρ_n of MgB_2 is fairly flat; the rise occurs mainly because of a drop in H_{c2} with T). This will lead to an insignificant rise in p_f even for a constant current. If the measurement is made with a constant-voltage source, p_f will actually drop with R (since then $p_f \propto V^2/R$ instead of $p_f \propto I^2R$). Our apparatus, when set to constant-voltage mode, has a source impedence as low as 0.3 Ohms which is about an order of magnitude below R_n. Thus the power dissipated doesn't rise rapidly with T. In the meanwhile the thermal properties that aid heat removal (conductivities and specific heat) become rapidly more effective as T increases, working strongly to prevent a runaway. Thus it is possible to make a quantitative evaluation of sample heating and the risk of thermal runaway.

A more detailed discussion on the subject of hot spots and thermal propagation in superconducting microbridges can be found in the review article by Gurevich and Mints[43] and references therein.

K. Depinning current versus depairing current

As long as gross sample heating or thermal runaway can be eliminated as discussed above, there is no confusion between the conventional (depinning) j_c and j_d. When j_d is exceeded, the resistance reaches the normal-state value R_n. When j_c is exceeded, the resistance approaches (if pinning is well overcome) the free-flux-flow value $R_f \sim R_nB/H_{c2}$. The latter is lower than R_n by three orders of magnitude. Hence the critical current measured is not just the conventional depinning threshold but a good estimate of j_d.

L. Uniformity of current flow

A superconducting wire with dimensions small compared to ξ and λ, automatically has a uniform distribution of j and $|\Delta|$ across the cross section. Close to T_c, ξ and λ diverge, so this condition applies to the T_{c2} shifts measured from resistive transitions at fixed currents (Eq. 22).

At lower temperatures and for sample cross sections that are not small, the question of current-flow uniformity needs to be further examined. In a type-I superconductor in zero applied field, the self flux is completely expelled and the current flows without resistance along the periphery of the cross section up to some threshold value. Resistance first appears when the self field at the surface exceeds H_c (Silsbee's rule). Beyond this the sample enters an intermediate state where normal regions coexist with superconducting ones and current flows through both so that the macroscopic resistance is a fraction of the normal-state value. In this intermediate state, the current is distributed more homogeneously over the sample volume.

In thin strips or bridges of type-II superconductors this process goes a step further. First, instead of H_c you have a much lower H_{c1} that defines the threshold of flux entry (possibly modified by surface barriers except for thin film bridges). Likharev[46] has shown that the minimum sample width for the nucleation of vortices is $4.4\xi(T)$. Second, because of the highly aspected geometry and consequent large demagnetization, the effective threshold is practically negligible. Thus there are always flux filled regions within bridges wider than the Likharev threshold. Also for the type-II case, vortices are present that necessarily move since we are concerned with current densities well beyond the depinning j_c. Hence the current flow will become homogeneous under these conditions. In general, as the current grows beyond j_c and the system becomes highly resistive, the current flow becomes macroscopically uniform as in a normal conductor. For a steady macroscopic state, the time averaged circulation of E vanishes so that its longitudinal value is constant across the width of the sample. In this case j will also be constant across the width, to the extent that the $j(E)$ funtion is independent of location. For a situation not far from equilibrium, the principle of minimum entropy production leads to the same conclusion.

This current-flow uniformity issue has been experimentally investigated by us in our previous work[22] on $Y_1Ba_2Cu_3O_7$ bridges of different widths. Fig. 5 shows $\rho(j)$ curves on two $Y_1Ba_2Cu_3O_7$ bridges measured in the highly non-linear mixed-state regime. Note that the resistivity changes by almost two orders of magnitude and

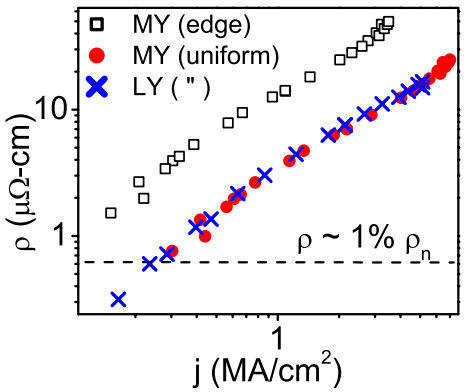

FIG. 5: Non-linear mixed-state response of two 90-nm thick $Y_1Ba_2Cu_3O_7$ microbridges. Samples MY and LY are 8 μm and 16 μm wide respectively. The lower two sets of symbols, showing ρ and j calculated assuming uniform current flow, are in excellent agreement. The open squares at the top, showing ρ and j (for MY relative to LY) based on an assumption of non-uniform current flow along edges, are in conspicuous disagreement. The dashed line corresponds to 1% of the normal-state resistivity. The measurements were made at $T = 50$ K and $B = 13.8$T ($\sim 20\%$ of H_{c2}); $\lambda \sim 200$ nm.

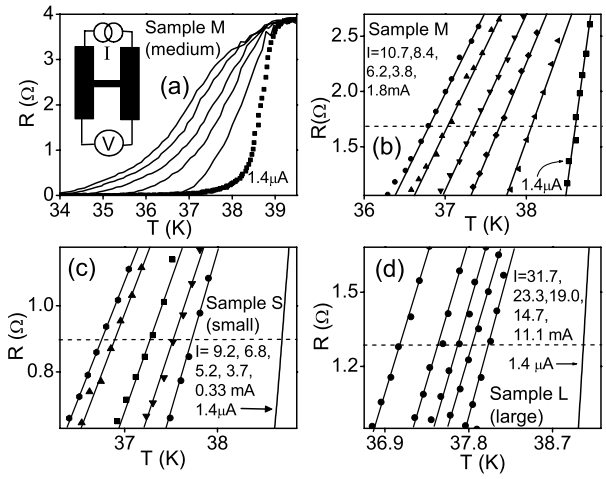

FIG. 6: Resistive transitions of MgB_2 bridges at different currents (values correspond to curves from left to right.). Panels (a) and (b) show two windows of the same data. The inset in (a) shows the sample geometry and configuration of leads. Panels (b), (c), and (d) show the central main portions of the transitions for three different sized samples. The rightmost curves at I=1.4 μA were measured with a continuous DC current; the rest used pulsed signals. The dashed lines represents $R = R_n/2$ for each sample. Reprinted with permission from M. N. Kunchur, S.-I. Lee, and W. N. Kang Phys Rev. B **68**, 064516 (2003). (c) (2003) The American Physical Society.

extends below 1% of ρ_n. The values of ρ and j calculated based on uniform current flow (i.e., dividing I by the nominal cross section to obtain j, etc.) are in excellent agreement. On the other hand if one assumes that the current flows non-uniformly along the edges, the nominal cross section will overestimate the actual area that contains the current. In this case, the relative error between samples MY and LY will be a factor of two in ρ and a factor of half in j (the sample widths differ by a factor of half). The edge flow assumption is checked by comparing the squares to the crosses. Clearly the assumption fails. We consider this to be definitive proof that the current does not just flow along the edges but occupies the whole sample cross section uniformly once the transport becomes dissipative. Other authors[5,47] have also reached the same conclusion that vortex motion homogenizes current flow.

It will be seen in the results below that the values of $j_d(0)$ in MgB_2 obtained from resistive-transition shifts near T_c agree with the values obtained at low temperatures from IV jumps. Also the values obtained for samples with different cross sections are all in mutual agreement. If the current flow did not fill the cross section, the macroscopically calculated value of j_d would be higher for a narrower sample. All of these observations confirm that current flow becomes homogeneous under dissipative conditions.

IV. RESULTS AND ANALYSIS

A. Resistive transitions at fixed currents

Fig. 6(a) shows the resistive transitions at different electric currents I for sample M. The inset shows the sample geometry. The horizontal sections of the current leads add a small (~ 15 %) series resistance to the actual resistance of the bridge. Because j in these wide regions is negligible, this resistance freezes out at the nominal unshifted T_c, making the onset seem to not shift. Similarly, the lower foot of the transition will have a flux-motion contribution $R_f \sim R_n B/H_{c2} < 5\%\ R_n$ from the self field. The central two-thirds portion of the transitions (magnified in panel (b)) circumvents these errors, displaying relatively parallel shifts due to pair breaking.

Variations in film thickness cause the transitions to broaden slightly with increasing j despite phase purity. For a simple model with series thickness variations δt, the functional shape of the current-dependent broadened transition is given by $R(j,T,\delta t) = R_n\{\log(j/4j_d(0)) - 1.5\log(1-T/T_c)\}/\log(1+\delta t/t)$, where δt=thickness variation. At the $R_n/2$ criterion (shown by the dashed line) the actual T_c shifts correspond exactly to shifts for a sample with the same mean thickness t but with $\delta t = 0$.

Panels (c) and (d) show similar sets of curves for two more samples. It should be noted that in addition to transition broadening due to thickness variations, the $R(T)$ transition may have some intrinsic width as a func-

tion of j. An analogous situation arises for $R(T)$ in a magnetic field, where there is an intrinsic broadening as B is increased[48]. Unfortunately there is no theoretical work on the $R(T)$ transition shape at high j. Nevertheless, we expect the midpoint criterion for the shifted T_c to provide a factor-of-two estimate of j_d. Fig. 7(a) shows the

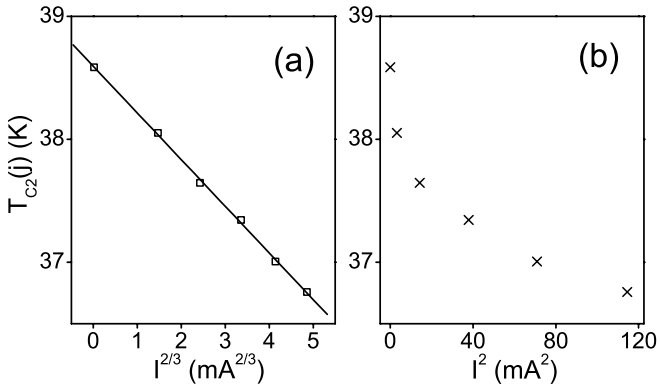

FIG. 7: Shifted transition temperatures at different currents. The two panels compare the same $T_{c2}(j)$ data versus $I^{2/3}$ and I^2, showing adherance to the $I^{2/3}$ law for pair breaking rather than the I^2 law for Joule heating. The linear fit (solid line) to the $I^{2/3}$ plot gives $I_d(0) = 257$ mA (see Eq. 22).

midpoint T_{c2}'s and their corresponding currents (ranging from 10^{-6} to 10^{-2} A) plotted as $I^{2/3}$ (expected for pair-breaking) and as I^2 (expected for Joule heating). The shifts are closely proportional to $I^{2/3}$ rather than to I^2, showing that heating is not appreciable (the plots for the other samples look similar). In fact from our earlier calculation of the thermal resistance, we can estimate the expected temperature rise. For the average $j \approx 0.4$ MA/cm^2, and transition-midpoint $\rho \approx 3\mu\Omega$-cm, we get $p \approx 0.5$ MW/cm^3. This heats up the sample by $\Delta T = pR_{th} \approx 6$ mK. This is much smaller than the size of the symbols on the plot and two orders of magnitude smaller than the observed shifts. Therefore heating is definitely negligible for the data shown in Fig. 7.

The slope $dI^{2/3}/dT_c(j)$ together with Eq. 22 gives a zero-temperature depairing current value of 257 mA (if the T_c criterion is taken at 30% and 70% of R_n, the corresponding I_d values are 196 mA and 299 mA respectively). Dividing this by the cross-sectional area gives $j_d(0)$. For samples S, M, N, and L the respective values of $j_d(0)$ are 2.2×10^7, 2.1×10^7, 2.0×10^7, and 1.8×10^7 A/cm^2. The four values are consistent within the uncertainties in the sample dimensions, implying a cross-sectionally uniform current density. As discussed earlier, this is especially expected close to the $T_{c2}(j)$ boundary where λ and ξ diverge and the superconductor becomes highly dissipative due to flux motion and fluctuations.

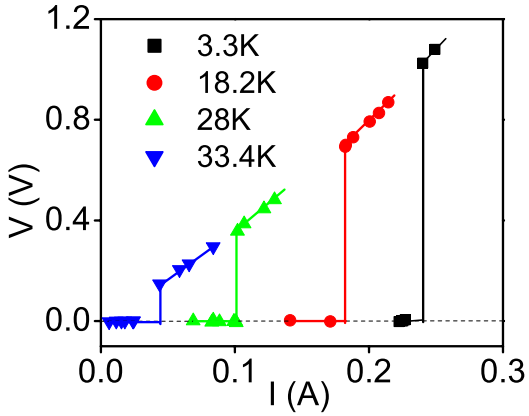

FIG. 8: IV curves for sample N at fixed temperatures (listed for curves going from right to left). Lines are drawn to guide the eye. Curves at intermediate temperatures were omitted for clarity. Beyond some threshold, the voltage jumps abruptly to the normal state. The slanted portions have the slope $V/I = R_n$ and their intercepts are zero.

B. Current-voltage curves at fixed temperatures

Fig. 8 shows current-voltage (IV) characteristics at various fixed temperatures for sample N (results for samples S, M, and L are similar). As I is increased, V remains close to zero until some threshold value. Above this it switches abruptly to the Ohmic behaviour $V = IR_n$. This threshold is a lower bound for I_d; however, as per our earlier discussion regarding thermal runaway, the temperature error is of the order of 1 K at low temperatures and negligible at higher temperatures. So the measured threshold can be associated with $I_d(T)$ at the nominal bath temperature.

For $T \gtrsim 35$ K the transition is gradual whereas at the lower temperatures it is rather abrupt[49]. This is partly because of film thickness variation as discussed earlier and partly because a type II superconducting phase transition changes from second order to first order at lower temperatures in the presence of a current[1].

The measurements on sample N were done with a signal source with a high source impedance thereby eliminating the "s" shape seen earlier in reference[49], where the external circuit had a source impedance comparable to that of the sample.

C. Zero-temperature values of j_d

From such IV characteristics measured at the lowest temperature the current required to drive the sample normal provides a direct estimate of $j_d(T \approx 0)$. These values of $j_d(0)$ for the four samples are shown in Table 1 (top row of numbers). These are seen to be consistent with the values (bottom row of numbers in Table 1) obtained from shifts in the resistive transitions near T_c (Fig. 7 and Eq. 22). It may be reiterated that the measurement does

Method:	Sample S	Sample M	Sample N	Sample L
IV at $T \ll T_c$	1.9×10^7	2.0×10^7	2.3×10^7	1.7×10^7
R(T) shift at $T \sim T_c$	2.2×10^7	2.1×10^7	2.0×10^7	1.8×10^7

Theory:	
GL	4×10^7
QPE shift	7×10^7

TABLE I: Zero-temperature values of j_d in A/cm^2

not reflect a depinning j_c; without significant pairbreaking or runaway heating, the motion of the minuscule self flux ($B \ll H_{c2}$) will produce $R_f \ll R_n$. The observed $R \approx R_n$ is reached only when the superconductivity is completely destroyed and the system has become normal.

The average value for all samples by both methods is $j_d(0) \approx 2 \pm 0.7 \times 10^7$ A/cm^2.

Our experimental estimate of $j_d(0)$ can be compared with theoretically calculated values from Eq. 21 and Eq. 28. The H_{c2} that enters these equations is the one that reflects the clean-limit BCS coherence length in the ab crystalline plane ($H \parallel c$ axis). An actual measured H_{c2} reflects the reduced coherence length due to scattering ($\xi \approx \sqrt{\xi_0 l}$). Hence j_d calculated from an empirically measured H_{c2} is going to be an overestimate. We take $H_{c2}(0) \approx 3$ T obtained from crystals by Sologubenko et al.[18] as an upper bound on the clean-limit H_{c2}. Because of sample to sample variation and different amounts of impurity scattering, the uncertainty and range in measured values of H_{c2}, span a factor of five[50]. For λ we take the value of 150 nm found using an AC induction technique on the same type of film samples by Kim et al.[20]. The experimental uncertainty and range in λ is about $\pm 40\%$[51], which is a tighter error bar than that of H_{c2}. With these values of H_{c2} and λ we obtain $j_d(0)$ based on the GL calculation (Eq. 21) and the quasiparticle-energy shift (Eq. 28). These calculated values are also shown in Table 1 and are indeed higher than the measured j_d (by about a factor of 2–3), but are of the same order of magnitude, which is about the best agreement that can be expected given the uncertainties in the parameters.

Incidentally, from the measured value[20] of 150 nm and Eq. 4, the superfluid density turns out to be $n_s(0) \approx 1.3 \times 10^{21}$ cm^{-3} and the measured[18] $H_{c2}(0) \approx 3$ T and Eq. 20 give $H_c \approx 0.18$ T.

D. Temperature dependence of I_d

We now take the I_d values determined by the IV jumps of Fig. 8 and plot them versus temperature. Fig. 9 shows such plots for two samples. The lines show the theoretical temperature dependencies expected from the GL treatment (Eq. 16) and from QPE shifts (Eq. 27). For $H_c(T)$ we take the generic empirical temperature dependence $H_c(T) \approx H_c(0)[1-(T/T_c)^2]$, for $\Delta(T)$ we take the BCS function, and for $\lambda(T)$ we take the empirical temperature dependence measured for MgB_2 by Kim et al. [3]. The ends of the curves [0,$I_d(0)$] and [$T_{c2}(0)$,0] are fixed. Other than that there are no adjustable parameters. As can be seen the data follow the general trend of the theoretical curves.

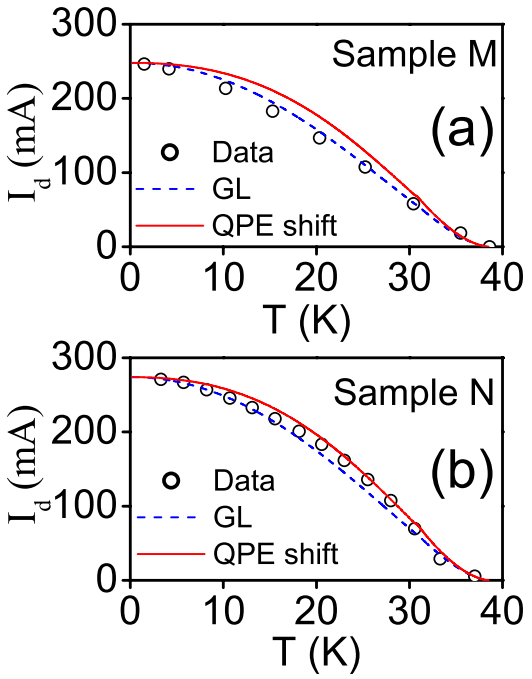

FIG. 9: Pair-breaking currents from IV characteristics at fixed temperatures (jumps in Fig. 8). The dashed line represents the GL $I_d(T)$ function (Eq. 17) and the solid line represents the theoretical $I_d(T)$ resulting from quasiparticle-energy shift (Eq. 27). The end points $I_d(0)$ and $T_{c2}(0)$ were fixed by the data; no other adjustable parameters are involved in the interpolation.

V. CONCLUSIONS

In conclusion, we have studied current induced pairbreaking in magnesium diboride over the entire temperature range for in-plane current transport. The measured $I_d(T)$ function is consistent with the expected theoretical temperature dependencies and conforms exactly to the $\Delta T_c \propto j^{2/3}$ behavior predicted near T_c. $j_d(0)$ obtained from the value of current required to drive the

[3] For our purpose and temperature range of interest ($0 \lesssim T \lesssim 0.95T_c$), Kim et al.'s empirical temperature dependence[20] of λ can be sufficiently well approximated by the simple function $\lambda(T) \approx \lambda(0)[1-(T/T_c)^{2.2}]^{-1/2}$ for $T < 0.8T_c$ and $\lambda(T) \approx 2.74\lambda(0)[1-(T/T_c)^{1.2}]^{-1/2}$ for $T > 0.8T_c$. Similarly the BCS temperature dependence of the gap can be approximated by $\Delta(T) \approx \Delta(0)[1-\tan(0.67396 \times (T/T_c)^{3.7})]$.

sample normal at $T \to 0$, agrees with the $j_d(0)$ deduced from the $\Delta T_c \propto j^{2/3}$ behavior close to T_c. The average value from our measurement is $j_d(0) \approx 2 \pm 0.7 \times 10^7$ A/cm^2, which is about a factor of three lower than the value $\sim 6 \times 10^7$ A/cm^2 calculated from published parameters, but the two are consistent within the uncertainities of the various parameters.

From a technological standpoint, the depairing current density of MgB_2 is about an order of magnitude lower than the high-T_c cuprates[52]. The good news is that flux motion in films is so quenched[53] that the depinning j_c at modest fields appears to be over 25% the magnitude of j_d[54–56], whereas for the cuprates, j_c and j_d can be separated by two or three orders of magnitude[21].

The tremendous experimental difficulties against measuring $j_d(0)$ until now, can be appreciated when one sees that for $Y_1Ba_2Cu_3O_7$ (where $j_d(T \approx T_c)$ was measured[52]) the power density would be[22,52] $\rho j^2 \sim 10^{-4}(10^8)^2 \sim 10^{12}$ W/cm^3!—hopelessly beyond our pulsed technique's limit of $\sim 10^{10}$ W/cm^3. Low-T_c materials like Nb and Pb also have prohibitive ρj^2 values. MgB_2's parameters ($\rho j^2 \sim 10^{-5}(10^7)^2 \sim 10^9$ W/cm^3) brought $j_d(0)$ within experimental reach.

VI. ACKNOWLEDGEMENTS

The author acknowledges useful discussions and other assistance from S. I. Lee, W. Kang, A. Gurevich, D. H. Arcos, G. Saracila, J. M. Knight, R. Prozorov, B. I. Ivlev, K. Gray, D. Larbalestier, and D. K. Finnemore. This work was supported by the U. S. Department of Energy through grant number DE-FG02-99ER45763.

* URL: `http://www.physics.sc.edu/kunchur`; Electronic address: `kunchur@sc.edu`

1. J. Bardeen, Rev. Mod. Phys. **34**, 667 (1962) and references therein.
2. V. P. Andratskii, L. M. Grundel, V. N. Gubanov, and N. B. Pavlov, Zh. Eksp. Teor. Fiz. **65**, 1591 (1973) [Sov. Phys.–JETP **38**, 794 (1974)].
3. W. J. Skcopol, Phys. Rev. B **14**, 1045 (1976).
4. J. Romijn, T. M. Klapwijk, M. J. Renne, and J. E. Mooij, Phys. Rev. B **26**, 3648 (1982).
5. A. Yu. Rusanov, M. B. S. Hesselberth, and J. Aarts, Phys. Rev. B **70**, 24510 (2004).
6. F. London and H. London, Proc. Roy. Soc. **A149**, 71 (1935).
7. Michael Tinkham, *Introduction to Superconductivity*, 2nd Edition (McGraw Hill, New York, 1996).
8. A. Gurevich, Phys. Rev. B **67**, 184515 (2003).
9. I. N. Askerzade, Physica C **390**, 281 (2003).
10. I. N. Askerzade, A. Gencer, N. Guclu, and A. Kihc, Supercond. Sci. Technol. **15**, L17 (2002).
11. M. Iavarone, G. Karapetrov, A. E. Koshelev, W. K. Kwok, G. W. Crabtree, D. G. Hinks, W. N. Kang, Eun-Mi Choi, Hyun Jung Kim, Hyeong-Jin Kim, and S. I. Lee, Phys. Rev. Lett. **89**, 187002 (2002).
12. P. C. Canfield and G. W. Crabtree, Physics Today, March issue, pg. 34 (2003).
13. K. Maki, Progr. Theor. Phys. **29**, 333 (1963).
14. Yu. N. Ovchinnikov, Zh. Eksp. Teor. Fiz. **56**, 1590 (1969) [Sov. Phys.–JETP **29**, 853 (1969)].
15. M. Yu. Kupriyanov and V. F. Lukichev, Fiz. Nizk. Temp. **6**, 445 (1980) [Sov. J. Low Temp. Phys. **6**, 210 (1980)].
16. W. N. Kang, H.-J. Kim, E.-M. Choi, C. U. Jung, S.-I. Lee, Science **292**, 1521 (2001).
17. W. N. Kang, E.-M. Choi, H.-J. Kim, and S.-I. Lee, Physica C **385**, 24 (2003).
18. A. V. Sologubenko, J. Jun, S. M. Kazakov, J. Karpinski, and H. R. Ott, Phys. Rev. B **65**, 180505(R) (2002).
19. M. N. Kunchur, C. Wu, B. I. Ivlev, Sung-Ik Lee, and W. N. Kang, Phys. Rev. B 68, 100503 (2003).
20. M.-S. Kim, J. A. Skinta, T. R. Lemberger, W. N. Kang, H.-J. Kim, E.-M. Choi, and S.-I. Lee, Phys. Rev. B **66**, 064511 (2002).
21. M. N. Kunchur, Mod. Phys. Lett. B. **9**, 399 (1995).
22. M. N. Kunchur, B. I. Ivlev, D. K. Christen, J. M. Phillips, Phys. Rev. Lett. 84, 5204 (2000).
23. M. N. Kunchur, Phys. Rev. Lett. **89**, 137005 (2002).
24. M. Nahum, S. Verghese, PL Richards, and K. Char, Appl. Phys. Lett. **59**, 2034 (1991), and references therein.
25. SK Gupta, P. Berdahl, RE Russo, G. Briceno, and A. Zettl, Physica C **206**, 335 (1993), and references therein.
26. M. Putti, V. Braccini, E. Galleani d'Agliano, F. Napoli, I. Pallecchi, A. S. Siri, P. Manfrinetti and A. Palenzona, Phys. Rev. B **67**, 064505 (2003).
27. T. Muranaka, J. Akimitsu, and M. Sera, Phys. Rev. B **64**, 20505 (2001).
28. E. T. Swartz and R. O. Pohl, Rev. Mod. Phys. **61**, 605 (1989).
29. W.J. Sichina, Perkin Elmer Instruments, Inc., Thermal Analysis application note. Web page: http://www.thermal-instruments.com/Applications/PETech-25.PDF
30. Meller Optics, Inc. Web page: http://www.melleroptics.com/datasheets/sapphire-3.htm
31. Ch. Walti, E. Felder, C. Degen, G. Wigger, R. Monnier, B. Delley, and H. R. Ott, Phys. Rev. B **64**, 172515 (2001).
32. R.K. Kremer, B.J. Gibson, and K. Ahn, http://arxiv.org/abs/cond-mat/0102432.
33. O. M. Stoll, S. Kaiser, R. P. Huebener, and M. Naito, Phys. Rev. Lett. **81**, 2994 (2001).
34. A. I. Larkin and Yu. N. Ovchinnikov, Zh. Eksp. Teor. Fiz. **68**, 1915 (1975) [Sov. Phys. JETP **41**, 960 (1976)].
35. L. E. Musienko, I. M. Dmitrenko, and V. G. Volotskaya, Pis'ma Zh. Eksp.Teor. Fiz. **31**, 603 (1980) [JETP Lett. **31**, 567 (1980)].
36. W. Klein, R. P. Huebener, S. Gauss, and J. Parisi, J. Low Temp. Phys. **61**, 413 (1985).
37. A. V. Samoilov, M. Konczykowski, N.-C. Yeh, S. Berry, C. C. Tsuei, Phys. Rev. Lett. **75**, 4118 (1995).
38. S. G. Doettinger, R. P. Huebener, R. Gerdemann, A. Kuhle, S. Anders, T. G. Trauble, and J. C. Villegier, Phys. Rev. Lett. **73**, 1691 (1994).
39. Z. L. Xiao and P. Ziemann, Phys. Rev. B **53**, 15265 (1996).

[40] A. I. Bezuglyj and V. A. Shklovskij, Physica C **202**, 234 (1992).
[41] A. I. Bezuglyj, Physica C **323**, 122 (1999).
[42] V. G. Voltskaya, N. E. Musienko, and I. M. Dmitrienko, Sov. J. Low Temp. Phys. **18**, 683 (1993).
[43] A. VI. Gurevich and R. G. Mints, Rev. Mod. Phys. **59**, 941 (1987).
[44] M. N. Kunchur and J. M. Knight, Mod. Phys. Lett. B **17**, 549 (2003).
[45] J. M. Knight and M. N. Kunchur, manuscript submitted to Phys. Rev. B (2004); preprint at http://www.physics.sc.edu/kunchur/papers/ep-relax.pdf.
[46] K. K. Likharev, Rev. Mod. Phys. **51**, 101 (1979).
[47] J. M. E. Geers, M. B. S. Hesselberth, J. Aarts, and A. A. Golobuv, Phys. Rev. B **64**, 94506 (2001).
[48] M. Tinkham, Phys. Rev. Lett. **61**, 1658 (1988).
[49] M. N. Kunchur, Sung-Ik Lee, and W. N. Kang, Phys Rev. B **68**, 064516 (2003).
[50] F. Simon, A. Jnossy, T. Fehr, F. Murnyi, S. Garaj, L. Forr,C. Petrovic, S. L. Bud'ko, G. Lapertot, V. G. Kogan, and P. C. Canfield, Phys. Rev. Lett. **87**, 47002 (2001).
[51] Y. Wang, T. Plackowski, A. Junod, Physica C **355**, 179 (2001).
[52] M. N. Kunchur, D. K. Christen, C. E. Klabunde, and J. M. Phillips, Phys. Rev. Lett. **72**, 752 (1994).
[53] D. H. Arcos and M. N. Kunchur, to be published; preprint at http://www.physics.sc.edu/kunchur/papers/absence.pdf.
[54] H.-J. Kim, W. N. Kang, E.-M. Choi, M.-S. Kim, K. H. P. Kim, and S.-I. Lee, Phys. Rev. Lett. **87**, 87002 (2001).
[55] S. H. Moon, J. H. Yun, H. N. Lee, J. I. Kye, H. G. Kim, W. Chung, and B. Oh, Appl. Phys. Lett. **79**, 2429 (2001).
[56] C. B. Eom, M. K. Lee, J. H. Choi, L. J. Belenky, X. Song, L. D. Cooley, M. T. Naus, S. Patnaik, J. Jiang, M. Rikel, A. Polyanskii, A. Gurevich, X. Y. Cai, S. D. Bu, S. E. Babcock, E. E. Hellstrom, D. C. Larbalestier, N. Rogado, K. A. Regan, M. A. Hayward, T. He, J. S. Slusky, K. Inumaru, M. K. Haas, and R. J. Cava, Nature **411**, 558 (2001).